Cancellation of the coherent accumulation in rubidium atoms excited by a train of femtosecond pulses

T. Ban, D. Aumiler, H. Skenderović, S. Vdović, N. Vujičić, and G. Pichler
Institute of Physics, Bijenička 46, Zagreb, Croatia

(Received 30 January 2007; revised manuscript received 14 June 2007; published 10 October 2007)

We investigated the coherence accumulation in Rb atoms excited by a train of femtosecond pulses. The coherence accumulation results in the velocity selective optical pumping of Rb hyperfine levels, observed by a cw probe laser. The effects of the pulse train excitation on the cw probe laser transmission were investigated, depending on the probe laser power. We observed the probe laser absorption increase in the strong probe case, followed by the reduction of the modulations in the probe laser absorption. Results show that accumulation of population and coherence can be effectively reduced and eventually destroyed by increasing the cw laser intensity. A strong cw laser can therefore serve as a switch from the pulse-train to pulse-by-pulse type of interaction of Rb atoms with the fs laser. We developed a density-matrix based theoretical model of the eight-level Rb atoms interacting with the fs and cw laser fields, and present agreement with the experimental results.

DOI: 10.1103/PhysRevA.76.043410 PACS number(s): 32.80.Qk, 42.50.Gy

I. INTRODUCTION

Mode-locked lasers generate short optical pulses by establishing a fixed phase relationship between all of the lasing longitudinal modes. For a train of identical pulses, separated by a fixed time interval, the spectrum can be obtained by a Fourier series expansion, yielding a comb of regularly spaced frequencies [1,2]. The optical frequencies f_n of the comb lines can be written as $f_n=nf_r+f_0$, where n is a large integer, f_r is the laser repetition rate, and f_0 is the carrier-envelope offset frequency. The comb's frequency spacing f_r can be measured straightforwardly and phase locked to an RF standard. In addition, the value of f_0 can be determined and controlled using different techniques [2]. The use of the phase-stabilized wide frequency-domain comb output of a femtosecond (fs) mode-locked laser has played a key role in recent advances in optical [3–6] and extreme ultraviolet frequency measurements [7–10], optical frequency synthesizers [11–13], and all optical atomic clocks [14–16].

The interaction of inhomogeneously broadened two-level atoms with a train of fs pulses was theoretically studied in Ref. [17]. Analytical results obtained for the case in which the atomic relaxation times are longer than the laser repetition period show the accumulation of population and coherence. Accumulative effects in the temporal-coherent control of three-level rubidium atoms excited by the fs frequency comb were investigated experimentally in Refs. [18,19]. The authors considered a sequence of pulse pairs separated by a laser repetition period, in which two pulses in the pair had temporal relative delay and showed that stimulated emission due to the accumulation of population in the excited state gives an important contribution to the coherently controlled processes.

The resonant interaction of the fs pulse train with cold rubidium atoms was investigated in literature [20–23]. The Jun Ye group developed direct frequency comb spectroscopy (DFCS) which uses light from a comb of appropriate structure to directly interrogate the atomic energy level structure and to study time-dependent quantum coherence [21]. In Ref. [22] DFCS is used for the determination of the absolute atomic transition frequencies anywhere within the comb bandwidth, for one- and two-photon processes in cold ^{87}Rb atoms. The $5S$-$7S$ two-photon transition is excited by scanning the offset frequency f_0 which eventually scans f_n, the optical frequency of the comb lines. The excited state population is determined from the $7S$-$6P$-$5S$ radiative cascade, whereby the blue photons at 420 nm are detected. In the case of the $5S_{1/2}$-$5P_{1/2}$ and $5S_{1/2}$-$5P_{3/2}$ one-photon transitions the fluorescence from the two $5P$ states was detected as the offset frequency f_0 is scanned. In Ref. [23] the authors show that the combination of pulse shaping with the fs comb increase the signal of a two-photon transition at a specific chirp while maintaining high resolution.

As we can see the theoretical work in [17] comprises fixed comb lines and broad absorption, while the work of the Jun Ye group relies on tunable frequency comb and narrow resonances. Our recent work [24,25] combines fixed comb lines, broad absorption (rubidium atoms at room temperature), and an additional cw scanning probe laser. Resonant excitation of the rubidium atoms by discrete frequency comb optical spectrum results in the comblike velocity distribution of the excited state hyperfine level populations and velocity-selective population transfer between the Rb ground state hyperfine levels. A modified DFCS was developed which uses the fixed frequency comb for the ^{85,87}Rb$5\,^2S_{1/2} \rightarrow 5\,^2P_{1/2,3/2}$ excitation and the weak cw scanning probe laser for ground levels population monitoring. Observed modulations in the probe absorption are a direct consequence of the velocity-selective optical pumping (VSOP) induced by the frequency comb excitation. The fs pulse train excitation of an Rb four ($5\,^2S_{1/2} \rightarrow 5\,^2P_{1/2}$) and six ($5\,^2S_{1/2} \rightarrow 5\,^2P_{3/2}$) level Doppler-broadened system was investigated theoretically in the context of the density matrix formalism. The analogous effect has also been observed and theoretically treated in the case of cesium atoms [26].

The present work improves the sensitivity of the detection by introducing the lock-in technique. This technique eliminates the Doppler background from the signal and results in

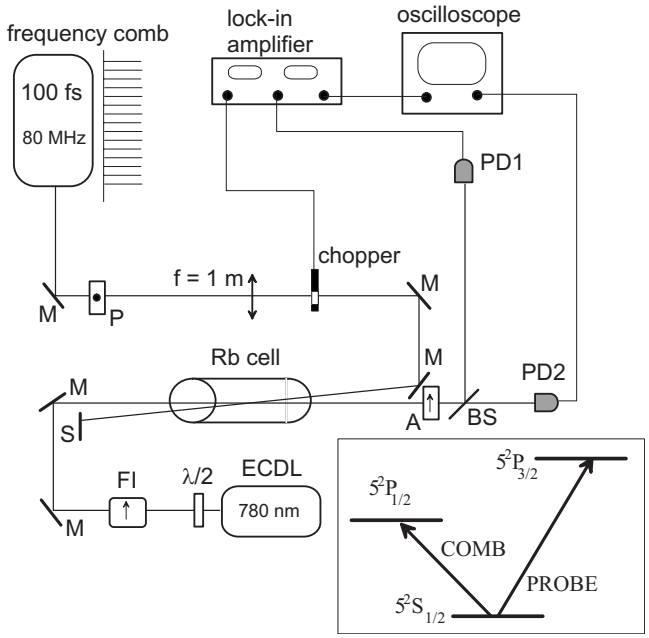

FIG. 1. Experimental scheme. PD: photodiode, P: polarizer, A: analyzer, FI: Faraday isolator, and S: beam stopper. Inset: relevant rubidium energy level scheme.

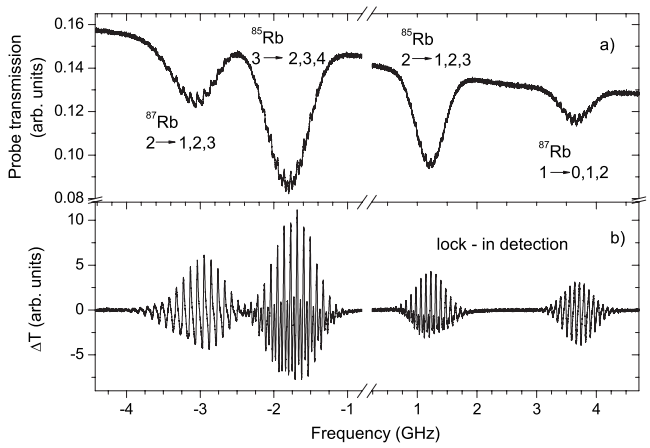

FIG. 2. (a) Measured probe transmission for the Rb vapor at room temperature in the case when the fs laser is tuned to $5\,^2S_{1/2} \rightarrow 5\,^2P_{1/2}$ transition at 795 nm. (b) fs laser induced modulations in the probe laser transmission measured with the lock-in amplifier technique. The probe laser frequency is continuously scanned across all four Doppler broadened $5\,^2S_{1/2} \rightarrow 5\,^2P_{3/2}$ absorption lines at 780 nm. The fs and probe laser powers are 600 mW and 2.6 μW, respectively.

direct monitoring of the modulation of the probe laser transmission. The structure and depth of the observed modulations are unique for each of the four Doppler broadened absorption lines and they reflect the structure of hyperfine levels and values of corresponding transition dipole moments. The enhanced sensitivity (over ten times) enables us to study various effects in frequency comb spectroscopy of Doppler broadened lines more thoroughly. In this work, we investigate how the frequency comb induced VSOP is influenced by the cw probe laser intensity. It turns out that in the strong probe regime the frequency comb excitation leads to the increase of the probe absorption and to the disappearance of the modulation structure. The disappearance of the modulation structure implies the disappearance of the VSOP. This imposes the conclusion that in the strong probe case, the atomic excitation is not driven by a pulse train, but rather by a pulse by pulse excitation. The physical mechanism behind this effect is the effective shortening of the atomic coherence relaxation time due to the strong probe laser. The numerical calculations of the density matrix evolution for this system, already developed in [24,25], are amended by introducing the probe laser electric field. Calculated probe laser absorption supports the experimental findings.

II. EXPERIMENT

The experimental arrangement, shown in Fig. 1, is similar to the one used in Ref. [25]. A Tsunami (Spectra Physics) mode-locked Ti:sapphire laser with pulse duration of about 100 fs generates ~5.8 THz broad optical frequency comb. It uses a rf synthesizer for active mode-locking by the use of an acousto-optic modulator. Besides this, the laser was not locked to any stable frequency reference, meaning no active stabilization of the laser repetition rate, f_r, and the carrier-envelope offset frequency f_0 was performed. However, the experimental spectra are taken in a time scale of about 5 s, during which the change in the repetition rate f_r, is negligible. In these conditions, we can say that the comb frequencies were not tunable and the frequency comb was kept constant during the measurements. The laser repetition rate f_r, measured with a fast photodiode amounts to 80 MHz.

The fs laser beam, chopped with a SR540 mechanical chopper at 3.5 kHz repetition rate, was weakly focused onto the center of the glass cell containing rubidium vapor at room temperature. The ^{85,87}Rb5 $^2S_{1/2}$ hyperfine ground state populations were monitored with a cw diode laser (Toptica DL100, ECDL at 780 nm), which propagated anticollinearly with the fs laser, intersecting it under a small angle in the center of the cell. The probe frequency was slowly scanned across the Doppler-broadened ^{85,87}Rb5 $^2S_{1/2} \rightarrow 5\,^2P_{3/2}$ hyperfine transitions at 3 GHz/s scanning rate. The probe laser transmission was simultaneously detected with two Hamamatsu Si photodiodes.

The signal from the second photodiode PD2 [shown in Fig. 2(a)] was directly fed into a digital oscilloscope (Tektronix TDS5140). It represents the transmission across all four Doppler broadened $5\,^2S_{1/2} \rightarrow 5\,^2P_{3/2}$ absorption lines at 780 nm for the fs laser tuned to $5\,^2S_{1/2} \rightarrow 5\,^2P_{1/2}$ transition at 795 nm. Two outer absorption lines result from the ^{87}Rb absorption, whereas the inner two come from ^{85}Rb absorption. The excited state $5\,^2P_{3/2}$ hyperfine levels are not resolved due to the Doppler broadening. Therefore each of the four absorption profiles consists of three Doppler broadened hyperfine transitions. The modulations of the absorption profiles are the result of the fs pulse train excitation of Rb atoms.

The signal from the first photodiode PD1 was fed to the lock-in amplifier (Stanford Research SR510) referenced to

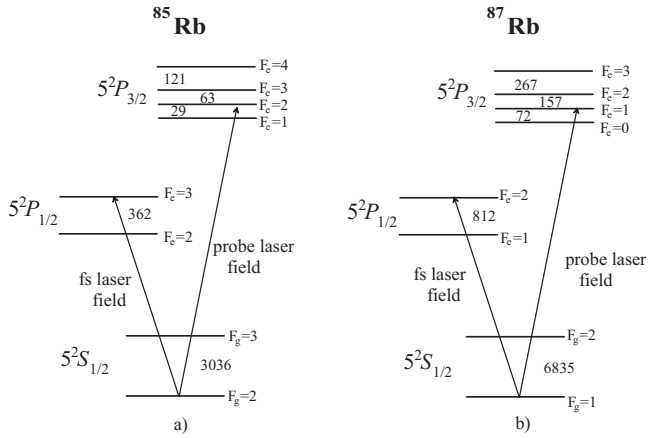

FIG. 3. Hyperfine energy level scheme of the ^{85,87}Rb $5\,^2S_{1/2}$, $5\,^2P_{1/2,3/2}$ eight-level system. The arrows indicate the fs and probe laser frequencies used in the theoretical calculation in the strong probe case.

the mechanical chopper on the fs laser beam. The lock-in signal represents the change of the probe laser transmission induced by the fs laser. The lock-in output [shown in Fig. 2(b)] is monitored on the digital oscilloscope. The signal in Fig. 2(b) represents $\Delta T = T_{\rm fs} - T$, where $T_{\rm fs}$ and T are the probe laser transmission with and without the fs pulse train excitation, respectively. The advantage of the lock-in detection technique is obvious, since the broad Doppler background is eliminated. Additionally, the signal-to-noise ratio is greatly enhanced providing insight to finer details of the modulations.

III. THEORY

A rubidium atom energy level scheme relevant for the experiment is given in Fig. 3. Theoretical modeling was carried out utilizing standard density-matrix analysis. The eight-level (two $5\,^2S_{1/2}$ hyperfine ground levels, two $5\,^2P_{1/2}$ and four $5\,^2P_{3/2}$ excited hyperfine levels) ^{85}Rb and ^{87}Rb atoms interacting with the fs and probe laser electric fields were considered.

The density matrix equations of motion are given by [27]

$$\dot{\rho}_{nm} = -i\hbar^{-1}[\hat{H},\hat{\rho}]_{nm} - \gamma_{nm}\rho_{nm}, \quad n \neq m, \tag{1}$$

$$\dot{\rho}_{nn} = -i\hbar^{-1}[\hat{H},\hat{\rho}]_{nn} + \sum_{m(E_m>E_n)} \Gamma_{nm}\rho_{mm} - \sum_{m(E_m<E_n)} \Gamma_{mn}\rho_{nn}, \tag{2}$$

where the subscripts nm refer to the eight hyperfine levels numbered from the lowest to highest energy level. Γ_{nm} gives the population decay rate from level m to level n. It includes level to level radiative decay and inelastic collisions. γ_{nm} is the damping rate of the ρ_{nm} coherence. The damping rates γ_{nm} for the off-diagonal elements of the density matrix are not independent of the damping rates of the diagonal elements. They are given by

$$\gamma_{nm} = \frac{1}{2}(\Gamma_n + \Gamma_m) + \gamma_{nm}^{\rm col}, \tag{3}$$

Γ_n and Γ_m denote the total population decay rates of level n and m, respectively. $\gamma_{nm}^{\rm col}$ is the dephasing rate due to the elastic collisions. The total population decay rate of level n, Γ_n, is given as a sum of the radiative decay rates $\Gamma_{n'n}$:

$$\Gamma_n = \sum_{n'(E_{n'}<E_n)} \Gamma_{n'n}. \tag{4}$$

In low density rubidium vapor at room temperature the radiative decay rates dominate all damping rates. The inelastic collisions contribute to the population and coherence decay through the thermalization process. Its rate is given by the product of the collision cross section [28], the average atom velocity, and the atomic number density. In our experimental conditions it is about 8 kHz. The elastic collisions contribute only to the decay of coherence (dephasing). The elastic collision dephasings are deduced from the experimental values for the self-broadening of Rb resonance lines [29]. For the rubidium vapor at room temperature they are about 16 kHz. The total radiative decay rates calculated from the lifetimes [30] of $5\,^2P_{1/2}$ (27.7 ns) and $5\,^2P_{3/2}$ (26.24 ns) are 36 and 38 MHz, respectively. As we can see, both elastic and inelastic decay rates are three orders of magnitude smaller than the radiative decay rates.

The Hamiltonian of the system is $\hat{H} = \hat{H}_0 + \hat{H}_{\rm int}$, where $\hat{H}_0$ is the Hamiltonian of the free atom and $(H_{\rm int})_{nm} = -\mu_{nm}E_T(t) - \mu_{nm}E_{\rm cw}(t)$ represents the interaction of the atom with the pulse train and cw laser electric field, μ_{nm} is the dipole moment of the electronically allowed $(F_g \rightarrow F_e = F_g, F_g \pm 1)$ transitions, calculated from Ref. [31]. Since in our experiment the frequency comb was centered on the $5\,^2S_{1/2} \rightarrow 5\,^2P_{1/2}$ transition and the probe laser was scanned across the $5\,^2S_{1/2} \rightarrow 5\,^2P_{3/2}$ transition, a single transition connecting two nm hyperfine levels is affected by just one of the two laser fields. The pulse train electric field is given by

$$E_T(t) = \left[\sum_{n=0}^{N} \varepsilon(t - nT_R)e^{in\Phi_R}\right] e^{i\omega_L t} = \varepsilon_T(t)e^{i\omega_L t}, \tag{5}$$

where N is a large integer (order of 10^6), $\varepsilon(t-nT_R)$ is the slowly varying envelope of the nth hyperbolic-secant laser pulse, Φ_R is the round-trip phase acquired by the laser within the cavity, T_R is the laser repetition period, and ω_L is the central laser frequency. $\varepsilon_T(t)$ is the slowly varying envelope of the pulse train. The pulse train frequency spectrum consists of a comb of N laser modes separated by $1/T_R$ and centered at $\omega_L + \Phi_R/T_R$. The nth mode frequency is given by $\omega_n = \omega_L + \Phi_R/T_R \pm 2\pi n/T_R$. The probe laser electric field is $E_{\rm cw}(t) = E_0 e^{i\omega_{\rm cw}t}$, where E_0 and $\omega_{\rm cw}$ are the amplitude and frequency of the monochromatic probe laser electric field.

From Eqs. (1) and (2) a system of 36 coupled differential equations for the slowly varying density-matrix elements was obtained. The population of the nth atomic level is given by the diagonal density-matrix element ρ_{nn}, whereas off-diagonal elements σ_{nm} represent the slowly varying envelope

of the coherences. The system of coupled differential equations was integrated using a standard fourth-order Runge-Kutta method.

IV. WEAK PROBE CASE

In the case of weak field approximation and linear absorption regime, the populations of the two ground levels are not noticeably altered by the interaction with the radiation field. Therefore for the probe laser intensities which are far below the saturation intensity for Rb $5\,^2S_{1/2} \rightarrow 5\,^2P_{3/2}$ transition (2.5 mW/cm^2 [30]), the influence of the probe laser on the ground levels population is negligible. Measured optical thickness is then directly proportional to the ground hyperfine level populations ρ_{11} and ρ_{22}, which are modified due to the $5\,^2S_{1/2} \rightarrow 5\,^2P_{1/2}$ fs pulse train excitation. In these conditions, the above described eight level system reduces to a four level system (two $5\,^2S_{1/2}$ ground and two $5\,^2P_{1/2}$ excited levels) interacting only with the pulse train electric field. This approach was extensively described in our previous papers [24,25]. The resulting system of ten coupled differential equations for slowly varying density-matrix elements was numerically solved and the time evolutions of the atomic level populations and coherences were obtained.

For the rubidium vapor at room temperature, the inhomogeneous Doppler broadening (of about 500 MHz) is significantly larger than the homogeneous broadening. Therefore the atomic transition frequency ω_{ge} must be replaced with $\omega'_{ge}=\omega_{ge}+\vec{k}\cdot\vec{v}$, where $\vec{k}$ is the laser wave vector and $\vec{v}$ is the atomic velocity. Different velocity groups correspond to different frequency detuning, $\delta=\vec{k}\cdot\vec{v}$, so for a given ω_n and a given $5\,^2S_{1/2}(F_g) \rightarrow 5\,^2P_{1/2}(F_e)$ hyperfine transition there is a velocity group (δ_n detuning), which fulfills the $\omega_n=\omega'_{ge}$ resonance condition. Since the pulse train frequency spectrum consists of a comb of laser modes separated by $1/T_R$ (80 MHz), the resonance condition is also satisfied for velocity groups with detuning $\delta=\delta_n \pm 2\pi k/T_R$, where k is a positive integer, corresponding to resonance with different comb modes. Therefore different velocity groups are in a different situation with respect to the excitation (accumulation) process, which leads to the VSOP of ground hyperfine levels and velocity selective comblike population in the excited hyperfine levels.

The experimental observation of the VSOP is achieved by monitoring the transmission of the weak cw probe laser scanning across all four $5\,^2S_{1/2} \rightarrow 5\,^2P_{3/2}$ Doppler broadened absorption lines. The calculated absorption coefficient for the rubidium vapor at room temperature interacting with the fs pulse train is shown in Figs. 4(a) and 4(b) for ^{87}Rb and ^{85}Rb isotopes, respectively. The calculations were performed for the fs laser electric field amplitude of 1.5×10^6 V/m and central fs laser frequency equal to ^{87}Rb $1 \rightarrow 1$ and ^{85}Rb $2 \rightarrow 2$ hyperfine transition frequencies. We calculated ^{85,87}Rb hyperfine ground level populations (ρ_{11} and ρ_{22}) at a time which corresponds to the mean interaction time of the atoms with the fs laser beam ($\tau=1.25$ μs). The calculation was performed for different atomic velocity groups (different detunings δ) and the velocity distributions of the ground state hyperfine level populations were obtained. Each hyperfine

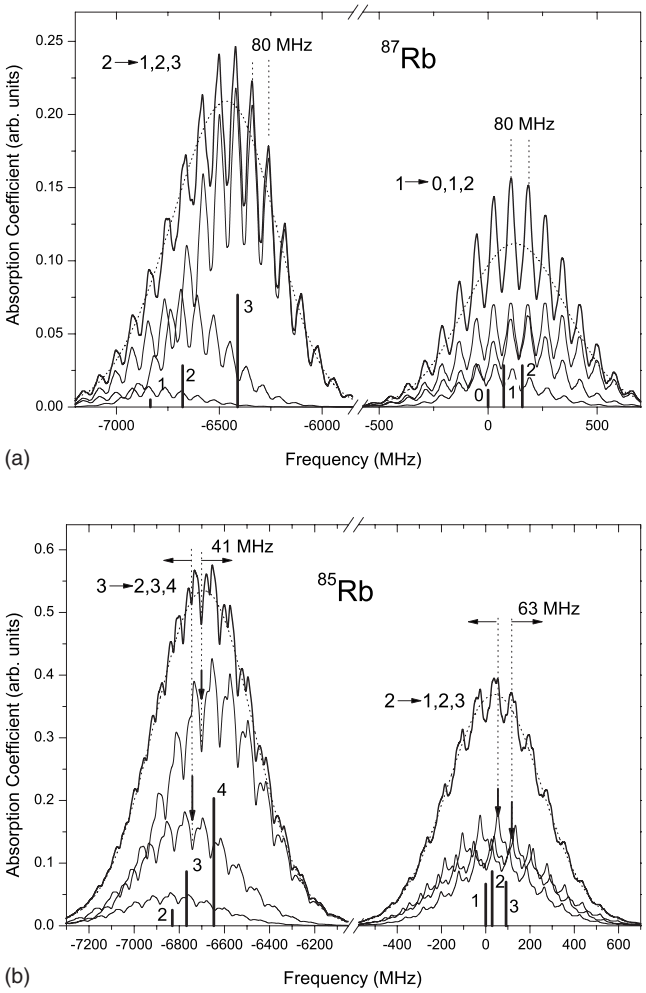

FIG. 4. Calculated optical thickness for ^{87}Rb (a) and ^{85}Rb (b) isotope in the case of $5\,^2S_{1/2} \rightarrow 5\,^2P_{1/2}$ fs laser excitation. An absorption line (thick line) is calculated by adding the contributions of three hyperfine components (thin lines). Doppler profiles are shown with dotted lines. Vertical lines denote the frequencies and relative transition dipole moments of hyperfine lines.

profile [shown with thin solid lines in Figs. 4(a) and 4(b)] was calculated as a convolution of the velocity distribution of the ground state population and the Lorentzian of natural width. The modulation in each hyperfine transition line is determined by the $5\,^2S_{1/2}$ and $5\,^2P_{1/2}$ hyperfine energy splittings and $5\,^2S_{1/2}(F_g) \rightarrow 5\,^2P_{1/2}(F_e)$ transition probabilities. The periodic behavior is given by the 80 MHz mode separation in the frequency comb. The difference in modulation structure for the case of ^{87}Rb and ^{85}Rb isotopes is explained in detail in our previous paper [25]. Each $5\,^2S_{1/2}(F_g) \rightarrow 5\,^2P_{3/2}(F_g, F_g \pm 1)$ absorption line [thick solid lines in Figs. 4(a) and 4(b)] is calculated by adding the contributions of three hyperfine components. If the frequency separation of the three hyperfine lines is favorable (close to the multiple of 80 MHz), the formed $5\,^2S_{1/2}(F_g) \rightarrow 5\,^2P_{3/2}(F_g, F_g \pm 1)$ absorption line exhibits stronger modulations, as seen in ^{87}Rb [Fig. 4(a)]. In the case of ^{85}Rb a two-peak modulation structure is observed [Fig. 4(b)] due to the more complex modulation structure of one hyperfine line and unfavorable $5\,^2P_{3/2}$

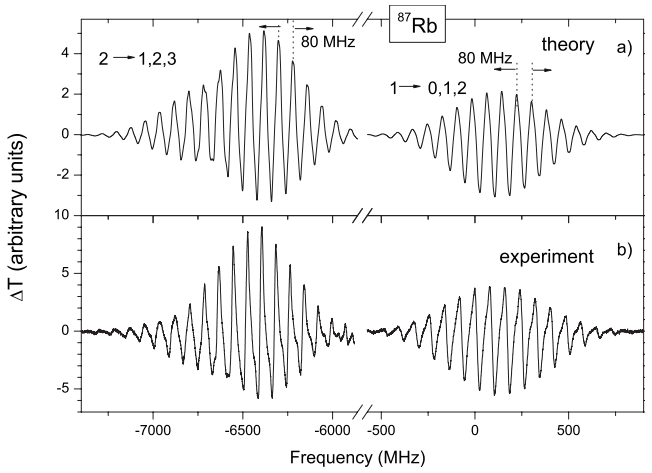

FIG. 5. Comparison between the calculated (a) and measured (b) ΔT for the ^{87}Rb isotope in the weak probe case. $\Delta T = T_{fs} - T$, where T_{fs} and T are the probe transmission with and without fs laser excitation. In the experiment the fs laser was adjusted at 795 nm with 600 mW of output power. The probe laser of 2.6 μW output power was scanned across $5\,^2S_{1/2} \rightarrow 5\,^2P_{3/2}$ absorption.

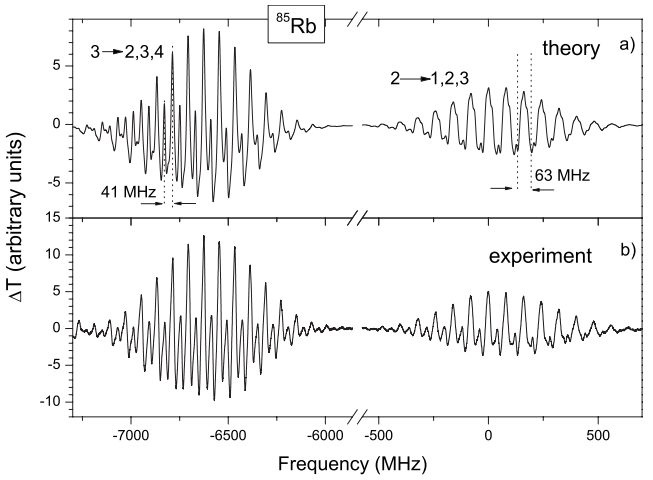

FIG. 6. Comparison between calculated (a) and measured (b) ΔT for the ^{85}Rb isotope in the weak probe case. $\Delta T = T_{fs} - T$, where T_{fs} and T are the probe transmission with and without fs laser excitation. In the experiment the fs laser was adjusted at 795 nm with 600 mW of output power. The probe laser of 2.6 μW output power was scanned across $5\,^2S_{1/2} \rightarrow 5\,^2P_{3/2}$ absorption.

hyperfine energy splittings. Although the overall absorption line is a result of adding three hyperfine lines, it is clear that some structures in the total absorption line can be predominately related to an individual hyperfine transition. Two minima in the ^{85}Rb $3 \rightarrow 2,3,4$ absorption line coincide with the minima in $3 \rightarrow 3$ and $3 \rightarrow 4$ hyperfine lines [indicated by arrows in Fig. 4(b)] which are detuned by 121 MHz. Due to the 80 MHz periodicity of the modulation structure in one hyperfine line, the 121 MHz detuning between two hyperfine lines yields 41 MHz detuned minima in the absorption line profile. The contribution of the $3 \rightarrow 2$ hyperfine line to the total absorption line is basically negligible due to the small transition dipole moment. In the formation of the $2 \rightarrow 1,2,3$ absorption line all three hyperfine lines contribute almost equally and it is difficult to assign the structure in the total absorption profile to a specific hyperfine transition. Two maxima denoted by arrows in Fig. 4(b) come predominately from maxima in the $2 \rightarrow 2$ and $2 \rightarrow 3$ hyperfine lines, and they are therefore detuned by 63 MHz. Calculated rubidium absorption lines in the case without a fs laser are shown in Fig. 4 by dotted lines.

In order to compare theory and experiment, calculated optical thickness and Beer Lambert law are used to simulate the probe laser transmission with (T_f) and without (T) the fs laser. By subtracting these two spectra, we simulate the change in the probe laser transmission due to the fs pulse train excitation, $\Delta T = T_{fs} - T$. Simulated and measured ΔT in the case of weak probe laser (probe power equal to 2.6 μW) scanning across all four $5\,^2S_{1/2} \rightarrow 5\,^2P_{3/2}$ absorption lines are shown in Figs. 5 and 6 separately for each isotope. The previously discussed two peak structure in the case of the ^{85}Rb isotope is now clearly visible in Fig. 6. The agreement between theory and experiment confirms this method as a high sensitivity technique for the frequency comb excitation processes monitoring. By monitoring ΔT, this technique enables us to study the influence of different experimental parameters (such as central fs laser wavelength and output powers of the fs and probe lasers) on the VSOP. We stress these results in the rest of the paper and give special attention to the set of measurements obtained for different probe laser output powers.

Structure and depth of the modulations in measured ΔT are strongly dependent upon the central wavelength of the fs laser. The modulations are strongest for the fs laser central wavelength tuned to resonance lines at 795 nm ($5\,^2S_{1/2} \rightarrow 5\,^2P_{1/2}$) and 780 nm ($5\,^2S_{1/2} \rightarrow 5\,^2P_{3/2}$). ΔT modulations decrease as the fs laser peak wavelength is detuned from the resonances. When the fs central wavelength is in the spectral region in-between the two resonances both resonances can be simultaneously excited due to the broad fs spectrum. The measurements of the modulations for the fs laser central wavelength tuned to 780, 795, and 787.5 nm are shown in Fig. 7. The fs laser spectral full width at half maximum was around 13 nm. Due to the different hyperfine energy splittings and the relevant transition dipole moments of the $5\,^2P_{1/2}$ and $5\,^2P_{3/2}$ excited states, a different modulation structure is observed when the fs laser is tuned to 780 and 795 nm.

Measured modulations for the ^{87}Rb $1 \rightarrow 0,1,2$ absorption line for a different fs laser central wavelength are shown in Fig. 8 in more detail. In the case of 795 and 780 nm resonant excitations the modulations show a similar single peak structure, relatively detuned by 36 MHz. As we discussed earlier, the one peak modulation structure in one modulation period of 80 MHz is directly connected to the excited state hyperfine energy splittings, which are close to a multiple of 80 MHz for both $5\,^2P_{1/2}$ (812 MHz) and $5\,^2P_{3/2}$ (72 and 157 MHz) excited states. The absolute frequency detuning of 36 MHz can be explained by inspecting the theoretical results for the optical thickness of the ^{87}Rb $1 \rightarrow 0,1,2$ absorption line profile in the case of 795 and 780 nm fs excitation, given in our previous paper [25]. In the calculations of the

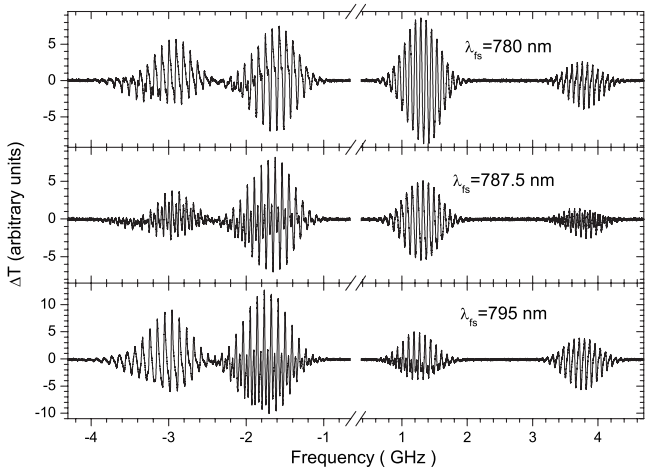

FIG. 7. Dependence of the modulation structure upon the central wavelength of the fs laser. The probe laser was scanned across $5\,^2S_{1/2} \rightarrow 5\,^2P_{3/2}$ absorption lines at 780 nm. fs and probe laser powers are 600 mW and 2.6 μW, respectively.

795 nm excitation the fs comb was set to be in resonance with the $5\,^2S_{1/2}(F_g=1) \rightarrow 5\,^2P_{1/2}(F_e=1)$ hyperfine transition, while in the case of the 780 nm the comb was set in resonance with the $5\,^2S_{1/2}(F_g=1) \rightarrow 5\,^2P_{3/2}(F_e=0)$ hyperfine transition. Taking into account the absolute frequencies of these two hyperfine transitions [30] the two independent combs can be related. This implementation results in the 36 MHz relative detuning between the calculated ^{87}Rb $1 \rightarrow 0,1,2$ absorption line modulation peaks in the case of 795 and 780 nm fs excitation. The most interesting result is obtained for the 787.5 nm fs excitation, where a double peak structure in one modulation cycle appears. This is a result of the broad frequency comb spectrum which at 787.5 nm central wavelength simultaneously excites both $5\,^2S_{1/2} \rightarrow 5\,^2P_{1/2,3/2}$ resonance lines. Therefore the double peak structure in 787.5 nm fs excitation is directly connected with one peak in 780 nm fs excitation and one peak in 795 nm fs

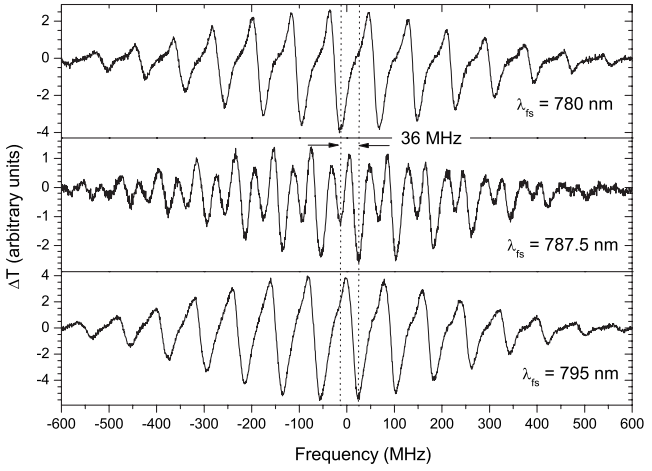

FIG. 8. Dependence of the modulation structure upon the central wavelength of the fs laser for the ^{87}Rb $1 \rightarrow 0,1,2$ absorption line, shown in more detail.

excitation. This leads to the conclusion that the absolute frequencies of laser modes in the frequency comb do not change when the central fs laser frequency is changed from 780 to 795 nm, which support excellent performance of the Tsunami mode-locked Ti:sapphire oscillator used in the experiment.

By changing the fs laser output power in the 50–800 mW power range, the structure of modulations in ΔT does not change significantly. The modulation depth increases linearly by increasing the fs laser output power and the saturation of the modulation intensities is observed for the fs laser power above 440 mW.

V. STRONG PROBE CASE

By increasing the cw probe laser power, the weak field approximation is not valid anymore and the complete theoretical treatment described in Sec. III must be applied. The model includes all eight hyperfine levels and the probe laser electric field is included explicitly in the interaction Hamiltonian. Time evolution of the density matrix elements is obtained by integration of 36 coupled differential equations. As an instructive example we show in Fig. 9 the time evolution of the ^{87}Rb ($5\,^2S_{1/2}, 5\,^2P_{1/2}, 5\,^2P_{3/2}$) hyperfine level populations for zero velocity group atoms, i.e., $\delta=0$. The calculations were performed for the 1.5×10^6 V/m fs laser electric field and fs laser central frequency set to a $5\,^2S_{1/2}(F_g=1) \rightarrow 5\,^2P_{1/2}(F_e=2)$ hyperfine transition. The probe laser frequency was set to a $5\,^2S_{1/2}(F_g=1) \rightarrow 5\,^2P_{3/2}(F_e=1)$ hyperfine transition frequency [indicated in Fig. 3(b)]. The hyperfine level population dynamics in the weak and strong probe case are calculated and shown in Figs. 9(a)–9(c) and Figs. 9(d)–9(f), respectively. The probe laser electric fields were set to 18 V/m in the weak probe case and to 300 V/m in the strong probe case. These values correspond to the experimental probe powers of 2.6 and 760 μW. In addition to the hyperfine level population dynamics, we show in Fig. 10 calculated time evolution of the slowly varying envelope of the coherence for the transition excited by the fs laser, in the case of weak and strong probe laser powers. Due to the fs resonant excitation the coherence is represented only by $\mathrm{Im}(\sigma_{14})$.

In the weak probe case the fractional ground and excited state populations exhibit the time evolutions equivalent to those presented in our previous work [24]. Two main processes dominate the atom dynamics: the hyperfine ground states optical pumping [decrease of ρ_{11} and simultaneous increase of ρ_{22}, Fig. 9(c)] and accumulation of the excited state population and coherence due to the pulse train excitation [see ρ_{44} and σ_{14} in Figs. 9(b) and 10]. Both processes are governed by the fs laser, whereas the probe laser influence is negligible. The optical pumping is a result of the excitation of the open two-level transition. The accumulation of population [Fig. 9(b)] and consequently the accumulation of coherence (Fig. 10) come as a result of the fs laser rubidium atom excitation, where the pulse repetition period T_R is smaller than the relaxation times of the system. Therefore the system can never completely relax between two consecutive laser pulses (see Ref. [17]). The pulse train excitation in the

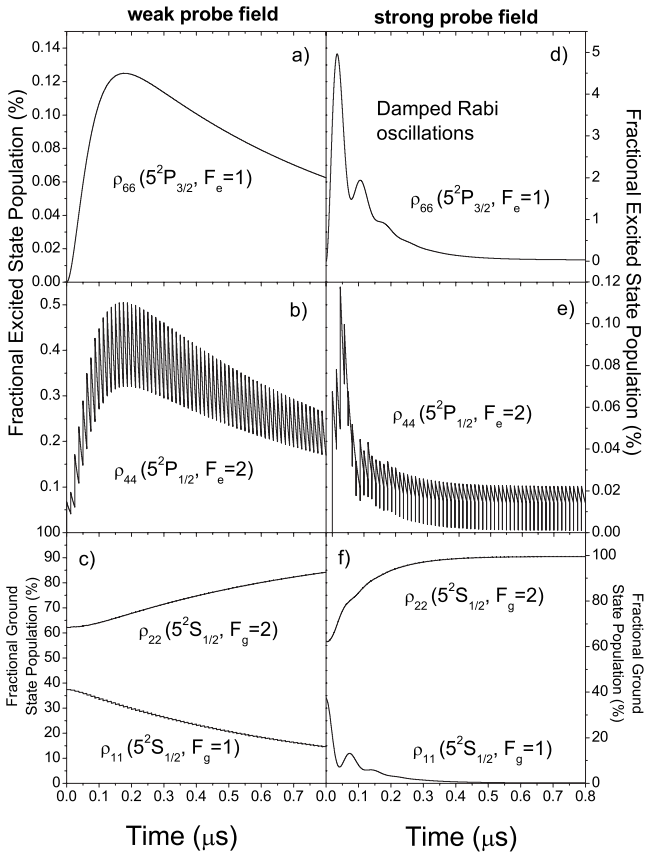

FIG. 9. Calculated time evolution of the ^{87}Rb ρ_{11}, ρ_{22} ground and ρ_{44}, ρ_{66} excited hyperfine level populations for zero velocity group atoms (δ=0) in the case of weak (18 V/m) and strong (300 V/m) probe fields. These probe powers correspond to 2.6 and 760 μW experimental probe powers, respectively. fs laser central frequency was set to $5\,^2S_{1/2}(F_g=1)\rightarrow 5\,^2P_{1/2}(F_e=2)$ hyperfine transition, while the probe laser frequency was set to $5\,^2S_{1/2}(F_g=1)\rightarrow 5\,^2P_{3/2}(F_e=1)$ hyperfine transition frequency [indicated in Fig. 3(b)].

time domain corresponds to the frequency comb excitation in the frequency domain. A steady state is achieved on a time scale of 3 μs with the $5\,^2P_{1/2,3/2}$ excited state populations less than 1%.

In the strong probe case the population time evolutions change significantly. The steady state is observed on a smaller time scale (around 0.7 μs). Strong optical pumping dominates the atom dynamics, but it is in this case governed predominately by the strong probe laser. The time evolution of the ρ_{11} and ρ_{66} populations show damped Rabi oscillations with Rabi frequency equal to 13.6 MHz, see Figs. 9(f) and 9(d). Although the $5\,^2P_{1/2}(F_e=2)$ hyperfine level is not directly connected with the probe laser excitation (it is excited by the fs laser), the influence of the probe laser on the ρ_{44} population and σ_{14} coherence is clearly visible from Figs. 9(e) and 10. Contrary to the weak probe case, in the strong probe case no accumulation of population and coherence induced by the fs laser excitation was observed. Since accumulation of population and coherence are typical pulse train effects [17], we can conclude that by increasing probe laser power the interaction of the system with the fs laser changes

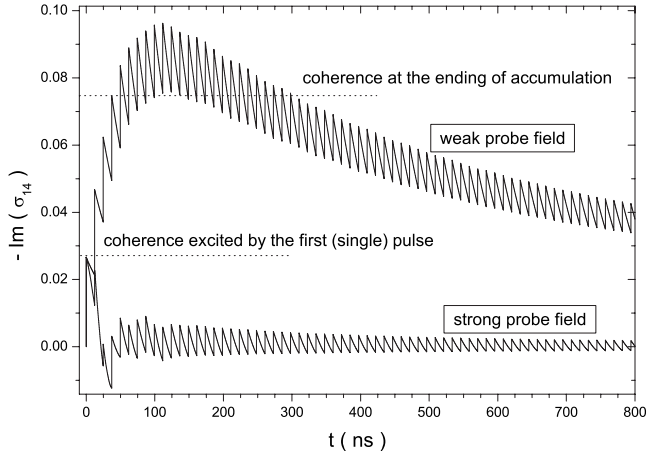

FIG. 10. Calculated time evolution of the slowly varying envelope of the coherence σ_{14} for the transition resonantly excited by the fs laser, in the case of weak (18 V/m) and strong (300 V/m) probe fields. fs laser central frequency was set to a $5\,^2S_{1/2}(F_g=1)\rightarrow 5\,^2P_{1/2}(F_e=2)$ hyperfine transition, while the probe laser frequency was set to a $5\,^2S_{1/2}(F_g=1)\rightarrow 5\,^2P_{3/2}(F_e=1)$ hyperfine transition frequency.

from the pulse train interaction to the pulse by pulse interaction. In other words, the effective atomic coherence relaxation time decreases when the probe power is increased. This is clearly evident by the inspection of the coherence induced by the first few pulses shown in Fig. 10. The change from pulse train interaction to pulse by pulse interaction in the time domain corresponds to the change from the frequency comb to the spectrum of the single pulse in the frequency domain. This leads to the conclusion that in the strong probe case, the atoms interact with the broad continuous spectrum of the single pulse and not with the frequency comb.

The probe laser absorption is calculated directly from the theoretical model. It is given by the imaginary part of the relevant off-diagonal density matrix element. Calculated ^{87}Rb $5\,^2S_{1/2}(F_g=1)\rightarrow 5\,^2P_{3/2}(F_e=1)$ probe laser absorption, for zero velocity group atoms, in the case of weak and strong probe fields is given in Fig. 11. The mean interaction time of Rb atoms with the fs laser is equal to τ=1.25 μs [24], so the probe absorption at time τ is considered. For small probe laser output power, Fig. 11(a), the probe absorption decreases when the fs laser is applied. As previously discussed, in this power regime the probe laser merely monitors ground levels population, i.e., the decrease of probe absorption corresponds to the decrease of the $5\,^2S_{1/2}(F_g=1)$ population. By introducing the fs laser into the vapor, a part of the ground $5\,^2S_{1/2}(F_g=1)$ level population is transferred to the ground $5\,^2S_{1/2}(F_g=2)$ state by fs laser induced optical pumping through the $5\,^2P_{1/2}$ state. In the strong probe case, Fig. 11(b), the effect of the fs laser on the probe absorption is opposite, the probe absorption increases when the fs laser is present in the vapor. This effect is a result of a strong probe laser which depletes the population of the ground $^2S_{1/2}(F_g=1)$ level and enhances the population of the ground $^2S_{1/2}(F_g=2)$ level by probe laser induced optical pumping through the $5\,^2P_{3/2}$ state. Although the central fs laser frequency is set to a

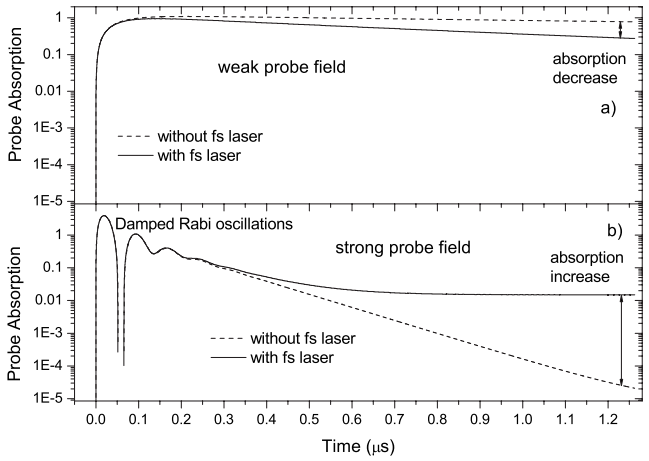

FIG. 11. Calculated probe laser absorption in the case of weak (a) and strong (b) probe laser fields with (solid lines) and without (dashed lines) the fs laser. In the case of a strong probe laser field the oscillations of the probe laser absorption due to Rabi oscillations (13.6 MHz for a given probe electric field and transition dipole moment) can be observed.

$5\,^2S_{1/2}(F_g=1)\rightarrow 5\,^2P_{1/2}(F_e=2)$ transition, the transfer of the ground $5\,^2S_{1/2}(F_g=2)$ level population to the excited $5\,^2P_{1/2}(F_e=1,2)$ levels is possible due to the broad fs frequency spectrum. The spontaneous decay from the $5\,^2P_{1/2}(F_e=1,2)$ levels then decreases the depletion of the ground $^2S_{1/2}(F_g=1)$ level population and therefore leads to the increase of the probe laser absorption in the presence of the fs laser.

The experimental investigation of the change in the probe transmission due to the fs laser excitation, $\Delta T=T_{\mathrm{fs}}-T$, for different probe laser powers is shown in Fig. 12. The fs laser was tuned to a $5\,^2S_{1/2}\rightarrow 5\,^2P_{1/2}$ transition at 795 nm and the average output power was 600 mW. The probe laser was scanned across all four $5\,^2S_{1/2}\rightarrow 5\,^2P_{3/2}$ absorption lines. The probe laser output power was increased gradually from

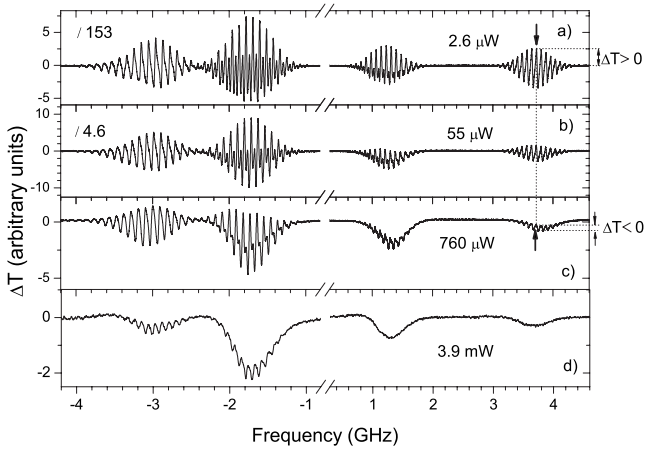

FIG. 12. The dependence of the probe laser transmission modulations ΔT on the probe laser output power. The fs laser is tuned to 795 nm, with 600 mW of average output power. The probe laser is scanned across $5\,^2S_{1/2}\rightarrow 5\,^2P_{3/2}$ absorption lines at 780 nm.

2.6 μW (weak probe case) up to 3.9 mW. By increasing the probe laser power the structure and depth of the modulations in ΔT change significantly. Two key points should be considered regarding the spectra shown in Fig. 12. First, the fs laser induced increase of the absorption for all velocity groups (ΔT negative for all four absorption lines) is observed in the strong probe case. In the case of ^{87}Rb $1\rightarrow 0,1,2$ and ^{85}Rb $2\rightarrow 1,2,3$ absorption lines, $\Delta T<0$ is observed for all velocity groups already at 760 μW probe laser power [Fig. 12(c)]. This experimental observation confirms the theoretical calculation shown in Fig. 11, where in the strong probe case the fs laser excitation leads to the increase of the probe absorption (corresponding to $\Delta T<0$). Second, as the probe laser power is increased the modulation depth decreases and a broad background with $\Delta T<0$ for all velocity groups appears. For the probe power of 3.9 mW, measured ΔT for ^{87}Rb $1\rightarrow 0,1,2$ and ^{85}Rb $2\rightarrow 1,2,3$ absorption lines result in a Doppler broadened absorption feature without the modulation structure [Fig. 12(d)]. The velocity selection due to the frequency comb excitation is therefore lost, and the atoms interact with individual pulses rather than with the pulse train. This result is supported by the theoretical calculation shown in Figs. 9(e) and 10 where in the strong probe case no accumulation of population and coherence is obtained.

VI. CONCLUSION

We have presented enhanced sensitivity measurements of the velocity selective optical pumping (VSOP) of the Rb ground state hyperfine levels induced by the pulse train excitation. Using this approach we were able to directly measure the change of the probe laser transmission as a result of the resonant fs laser excitation of the Rb atoms. The results of this experimental method in the case of the weak probe laser output power are verified by the theoretical treatment developed in our previous papers. The agreement between theory and experiment is satisfactory, confirming this method as a high sensitivity technique for the frequency comb excitation processes monitoring. This allowed us to study the VSOP under different experimental conditions.

The most interesting result has been obtained in the case of the strong probe laser field. In this case, the velocity selection due to the frequency comb excitation is lost, corresponding to the interaction of atoms with the individual pulses rather than with the pulse train. The effects of the fs laser excitation on the strong probe laser absorption are calculated by applying an extended theoretical model. Calculated results confirm the experimental findings. The strong probe laser field decreases the effective coherence relaxation time of the Rb system leading to the pulse by pulse excitation. Therefore by changing the probe laser power, a gradual change from the frequency comb excitation to the pulse by pulse excitation of Rb atoms is observed. This result could lead to the application in the coherent control experiments [32]. The authors in Ref. [17] demonstrated the necessity of considering accumulative effects for a full explanation of a coherent control signal obtained from the rubidium vapor. In order to avoid the typical pulse train effects while still preserving high repetition frequency of the pulses our method could be applied.

Exploitation of quantum memory for information storage and data processing is one of the fundamental aspects in the experimental physics [33,34]. In the experiments where the coherence of the system has to be controlled and maintained for as long a time as possible despite higher field intensities [35], our method could be applied for system coherence monitoring.

In addition, the applied laser scheme (strong probe case) could be correlated to the V-type electromagnetically induced transparency (EIT) scheme [36], where the strong cw laser acts as a pump laser and the frequency comb represents an array of the weak probe lasers. However, to observe the EIT resonance in such a scheme the absorption of an individual frequency comb mode has to be measured. This is an additional experimental challenge which will be treated in future experiments.

ACKNOWLEDGMENTS

We acknowledge the support from the Ministry of Science Education and Sports of the Republic of Croatia (Project No. 035-0352851-2857) and Alexander Von Humbolt Foundation (Germany). Interest and support by Professor K.-L. Kompa is gratefully acknowledged.

[1] S. T. Cundiff and J. Ye, Rev. Mod. Phys. **75**, 325 (2003).
[2] J. Ye and S. T. Cundiff, *Femtosecond Optical Frequency Comb Technology* (Springer, Boston, 2005).
[3] Th. Udem, J. Reichert, R. Holzwarth, and T. W. Hänsch, Phys. Rev. Lett. **82**, 3568 (1999).
[4] J. Ye, T. H. Yoon, J. L. Hall, A. A. Madei, J. E. Bernard, K. J. Siemsen, L. Marmet, J.-M. Chartier, and A. Chartier, Phys. Rev. Lett. **85**, 3797 (2000).
[5] M. Niering, R. Holzwarth, J. Reichert, P. Pokasov, Th. Udem, M. Weitz, and T. W. Hänsch, Phys. Rev. Lett. **84**, 5496 (2000).
[6] Th. Udem, S. A. Diddams, K. R. Vogel, C. W. Oates, E. A. Curtis, W. D. Lee, W. M. Itano, R. E. Drullinger, J. C. Bergquist, and L. Hollberg, Phys. Rev. Lett. **86**, 4996 (2001).
[7] S. Witte, R. Th. Zinkstok, W. Ubachs, W. Hogervorst, and K. S. E. Eikema, Science **307**, 400 (2005).
[8] R. J. Jones, K. D. Moll, M. J. Thorpe, and J. Ye, Phys. Rev. Lett. **94**, 193201 (2005).
[9] S. Hannemann, E. J. Salumbides, S. Witte, R. Th. Zinkstok, E.-J. Van Duijin, K. S. E. Eikema, and W. Ubachs, Phys. Rev. A **74**, 012505 (2006).
[10] S. Hannemann, E. J. Salumbides, S. Witte, R. Th. Zinkstok, E.-J. Van Duijin, K. S. E. Eikema, and W. Ubachs, Phys. Rev. A **74**, 062514 (2006).
[11] S. T. Cundiff, J. Ye, and J. L. Hall, Rev. Sci. Instrum. **72**, 3749 (2001).
[12] R. Holzwarth, Th. Udem, T. W. Hänsch, J. C. Knight, W. J. Wadsworth, and P. St. J. Russell, Phys. Rev. Lett. **85**, 2264 (2000).
[13] J. D. Jost, J. L. Hall, and J. Ye, Opt. Express **87**, 270801 (2001).
[14] S. A. Diddams *et al.*, Science **293**, 825 (2001).
[15] J. Ye, L. S. Ma, and J. L. Hall, Phys. Rev. Lett. **87**, 270801 (2001).
[16] A. D. Ludlow *et al.*, Phys. Rev. Lett. **96**, 033003 (2006).
[17] D. Felinto, C. A. C. Bosco, L. H. Acioli, and S. S. Vianna, Opt. Commun. **215**, 69 (2003).
[18] D. Felinto, L. H. Acioli, and S. S. Vianna, Phys. Rev. A **70**, 043403 (2004).
[19] D. Felinto, C. A. C. Bosco, L. H. Acioli, and S. S. Vianna, Phys. Rev. A **64**, 063413 (2001).
[20] M. J. Snadden, A. S. Bell, E. Riis, and A. I. Ferguson, Opt. Commun. **125**, 70 (1996).
[21] A. Marian, M. C. Stowe, J. R. Lawall, D. Felinto, and J. Ye, Science **306**, 2063 (2004).
[22] A. Marian, M. C. Stowe, D. Felinto, and J. Ye, Phys. Rev. Lett. **95**, 023001 (2005).
[23] M. C. Stowe, F. C. Cruz, A. Marian, and J. Ye, Phys. Rev. Lett. **96**, 153001 (2006).
[24] D. Aumiler, T. Ban, H. Skenderović, and G. Pichler, Phys. Rev. Lett. **95**, 233001 (2005).
[25] T. Ban, D. Aumiler, H. Skenderović, and G. Pichler, Phys. Rev. A **73**, 043407 (2006).
[26] N. Vujičić, S. Vdović, D. Aumiler, T. Ban, H. Skenderović, and G. Pichler, Eur. Phys. J. D **41**, 447 (2007).
[27] R. W. Boyd, *Nonlinear Optics* (Academic Press, San Diego, 2003).
[28] C. Cohen-Tannondji and A. Kastler, Prog. Opt. **V**, 3 (1966).
[29] W. Demtröder, *Laser Spectroscopy* (Springer-Verlag, Berlin, 2003).
[30] D. A. Steck, *Rubidium 87 D Line Data*, http://steck.us/alkalidata.
[31] O. Axner, J. Gustafsson, N. Omenetto, and J. D. Winefordner, Spectrochim. Acta, Part B **59**, 1 (2004).
[32] A. H. Zewail, *Femtochemistry: Ultrafast Dynamics of the Chemical Bond* (World Scientific, Singapore, 1994).
[33] J. Ahn, T. C. Weinacht, and P. H. Bucksbaum, Science **287**, 463 (2000).
[34] D. Kielpinski *et al.*, Science **291**, 1013 (2001).
[35] A. Nazarkin, R. Netz, and R. Sauerbrey, Phys. Rev. Lett. **92**, 043002 (2004).
[36] M. D. Lukin, Rev. Mod. Phys. **75**, 457 (2003).